DEM MODELLING OF A JOINTED ROCK BEAM WITH EMPHASIS ON INTERFACE PROPERTIES

C.W. Boon [a], G.T. Houlsby [a] and S. Utili [b]

[a] *Department of Engineering Science, Oxford University, Parks Road, Oxford OX1 3PJ, UK*

[b] *School of Engineering, University of Warwick, Coventry CV4 7AL, United Kingdom*

Abstract

In this paper, a comparison is made between the results obtained by Tsesarsky & Talesnick (2007) using the finite difference software (FLAC) and our analyses performed via the distinct element method (DEM) employing rigid blocks and compliant joints. We then examine the capability of rigid-block DEM at modelling joints realistically, with emphasis on the moment transfer between blocks. The line of thrust from our analysis was found to fit well with the well established uniform catenary curve (Timoshenko, 1983) and the parabola which has been used extensively in the rock engineering literature (Beer & Meek, 1982; Sofianos, 1996; Brady & Brown, 2004). This is an important verification exercise that is still lacking in the literature, especially for rigid block DEM. Finally, a comparison is made between the experiment carried out by Talesnick et al. (2007) and the DEM. The laboratory data of Talesnick et al. (2007) were reinterpreted to derive more accurate contact laws in both normal and shear directions. A strain-hardening or continuously yielding model was adopted in the latter. The approach of calibration was demonstrated. Our numerical findings suggest that improved predictions of the beam deflections can be obtained. The predicted horizontal thrusts are comparable to the results obtained by FLAC.

Keywords: DEM; shear stiffness; centrifuge model; jointed beam; voussoir beam; irrecoverable-closure; plastic displacements

1. Introduction

To predict deformations within a jointed rock mass, it is necessary to adopt accurate contact models for the rock joints. However in the literature there is still a lack of validated approaches for jointed rock masses with more than a joint. The merits of adopting an accurate contact model and a reliable contact detection algorithm in the Distinct Element Method (DEM) are demonstrated through simulating a well instrumented laboratory-scale experiment on a single layer jointed beam (called voussoir beam) carried out by Talesnick et al. (2007) in a centrifuge. The approach illustrated here can be applied to several engineering problems in rock mechanics, e.g. tunnelling (Boon et al., 2014a) and rock slope stability (Boon et al., 2014b).

The influence of jointing has been studied by adopting an equivalent rock mass elastic modulus (Diederichs & Kaiser, 1999b), or through semi-analytical solutions based on an empirical databases developed from numerical simulations (Nomikos et al., 2002; Tsesarsky, 2012). To account for the influence of jointing more directly, several investigators have used discontinuum analysis, i.e. the DEM or DDA (Tsesarsky & Hatzor, 2006; Tsesarsky et al, 2007; Hatzor & Benary, 1988; Hatzor et al., 2010; Barla et al., 2010), but these studies have been limited until now to simple contact models between rock joints.

Talesnick et al. (2007) measured the horizontal thrust and the vertical deflection of a voussoir beam subject to increasing levels of gravitational acceleration. Then, Tsesarsky & Talesnick, (2007) ran numerical simulations of the beam using the finite difference method (FDM) and DDA. They found that, for both FDM and DDA, the horizontal thrusts were underpredicted, inter-block slip was underpredicted, and the block rotations were uniform compared to the experimental measurements in which rotation was greatest at the abutment blocks and least at the midspan blocks. Furthermore, deflections were

underpredicted (the smallest measured deflection profile among the three tests carried out in Talesnick et al. (2007) was used for as a benchmark case in Tsesarsky & Talesnick et al. (2007)).

This paper presents distinct element method (DEM) simulations that allowed obtaining better estimates of the deflections for these centrifuge tests. The open-source DEM academic code YADE (Kozicki & Donzé, 2008) was employed for our study together with the new contact detection algorithm recently proposed by Boon et al. (2012). Second, the robustness of using DEM to model problems involving moment transfers between non-deformable blocks with compliant contacts is investigated.

2. Numerical setup

The centrifuge model of Talesnick et al. (2007) consisted of six equal Gypsum blocks, flanked by two fixed larger abutment blocks. Two opposing sides of each block were fitted with standard abrasive paper. Two prism dimensions were used: 46 x 46 46 mm and 46 x 46 x 23 mm, herein referred to as the full-block and half-block beam respectively. The properties of the blocks are listed in Table 1. An initial horizontal force of approximately 60 N was applied to the blocks at 1 g. Gravity was gradually increased up to 40 g for the full-block beam and 90 g for the half-block beam.

The same loading sequence was applied in our DEM simulations. Also, we used the experimentally derived contact laws reported by Tsesarsky & Talesnick (2007), for sake of comparison with their numerical results. Concerning the stress-dependent stiffness in the normal direction, a contact model with the stiffness being a linear function of the exchanged normal stresses fits the experimental data best. This model can be expressed as (Tsesarsky & Talesnick, 2007):

$$k_{\mathrm{n}} = \frac{\mathrm{d}\sigma_{\mathrm{n}}}{\mathrm{d}u_{\mathrm{n}}} = 4\times10^{9} + 7.4\times10^{4}\sigma_{\mathrm{n}} \text{ (units: Pa)} \quad (1)$$

$$k_{\mathrm{s}} = 1\times10^{8} + 9.7\times10^{4}\sigma_{\mathrm{n}} \quad (2)$$

3. A new contact model from reinterpretation of the experimental measurements of (Talesnick et al., 2007)

Expressing the contact model as a stress-displacement function is convenient for DEM calculations since the overlap distance between blocks is the input for the contact model. Therefore, integrating Eq. (1), we obtain:

$$\sigma_{\mathrm{n}} = 0.5405\times10^{5}(\mathrm{e}^{7.4\times10^{4}u_{\mathrm{n}}} - 1) \quad (3)$$

To improve predictions, we reinterpreted the experimental data of Talesnick et al. (2007) and Talesnick (2007) to derive more accurate normal and shear contact models. The normal stress-displacement relationship for the joints can be derived directly from the experimental stress-displacement data (see Figure 1(a)) of uniaxial compression tests run by Talesnick et al. (2007) on a three-block column. This approach is more direct than working out the stiffnesses from the slope of the curve as done in Tsesarsky & Talesnick (2007) (Eq. (1)).

In a three-block column, there are two rock joint contacts plus one equivalent rock joint contact counting the two block interfaces at the two ends of the column in contact with the abutments. The deformations of the intact material were calculated assuming linear elastic behaviour for the intact blocks and a Young's modulus of 5600 MPa (see Table 1). The deformations due to the joints were then deduced by subtracting the deformations of the intact material from the total measured deformations. As shown in Figure 1(b), the stiffness

relationship proposed by Tsesarsky & Talesnick (2007) in Eq. (3) is less accurate. As a first estimate, the normal stiffness for the linear model in Eq. (3) is halved, so that:

$$\sigma_{\mathrm{n}} = 0.5405\times10^{5}\left(\mathrm{e}^{3.7\times10^{4}u_{\mathrm{n}}}-1\right) \tag{4}$$

From Figure 1(b), it emerges that the stress-displacement response given by Eq. (4) matches the experimental measurements well.

From the data reported in Talesnick (2007) it is apparent that the joint shear stiffness measured in the centrifuge decreases with shear displacement (see Figure 2). However shear stiffness degradation is not captured by the equation proposed by Tsesarsky & Talesnick, (2007) (Eq. (2)) that reflects the initial (high) shear stiffness only and therefore leads to an underestimation of the shear displacements. The instantaneous shear stiffness can be modeled as:

$$k_{\mathrm{s}} = \left(1-\frac{u_{\mathrm{s}}}{u_{\mathrm{peak}}}\right)k_{\mathrm{s\_initial}}, \qquad u_{\mathrm{s}} < u_{\mathrm{peak}} \tag{5}$$

where $k_{\mathrm{s\_initial}}$ is the initial shear stiffness, u_{s} is the shear displacement, and u_{peak} is the displacement at which the shear stress reaches its peak. u_{peak} (intercepts of the lines with the x-axis in Figure 2) can be assumed as:

$$u_{\mathrm{peak}} = 2\times10^{-6}\sigma_{\mathrm{n}}^{0.213} \tag{6}$$

while the initial shear stiffness, $k_{\mathrm{s\_initial}}$, can be modeled as (obtained by fitting a curve for the data points in Figure 3 to match the y-intercept of Figure 2):

$$k_{\mathrm{s\_initial}} = 1.9\times10^{6}\sigma_{\mathrm{n}}^{0.7} \tag{7}.$$

For high normal stresses, the initial shear stiffness predicted using Eq. (7) is lower compared to the linear model (Eq. (2)) proposed by Tsesarsky & Talesnick (2007) (Figure 3). The model

predictions for the instantaneous shear stiffness juxtaposed against experimental measurements are shown in Figure 3(b).

In the case of complex stress paths, it is possible that this model (Eq. (5)) may give zero stiffness before yielding occurs; e.g. if the normal stress increases as the joint shears, the joint may experience $u_s \geq u_{peak}$ although the shear stress is still less than $\mu\sigma_N$ where μ is the joint friction coefficient. This behaviour is not physically sound. Rather than modeling stiffness degradation, it is numerically more robust to model this behavior as strain hardening or continuous yielding so that:

$$\mu = \mu_0(1 - e^{-u_s/u_{peak}}) \tag{8}$$

where μ_0 is the maximum friction coefficient, i.e. 40°. In this shear model, the friction coefficient increases from zero with shear displacement and the elastic shear stiffness is simply $k_{s\_initial}$. The stress-update algorithm for the DEM is explained in Appendix A. Figure 4 shows that Eq. (8) predicts the laboratory measurements well.

4. Results

4.1 Comparison against FLAC simulations (Tsesarsky & Talesnick, 2007)

The same values of joint stiffness as those adopted in Tsesarsky & Talesnick's FDM simulations (see Table 2) were employed in our DEM simulations. In two of the three simulations, the stiffness was assumed constant, whilst in another simulation a linearly varying stiffness was adopted according to the contact law of Eqs. (2) and (3). The horizontal thrusts obtained from our DEM simulations for the full-block beam together with the values obtained by FDM analyses of Tsesarsky & Talesnick (2007) are shown in Figure 5. The comparisons consisting of the midspan deflections are shown in Table 2 and one of the

obtained deflection profiles is plotted in Figure 6. Differences in block rotations, i.e. greater for the blocks at the abutment than at the midspan, are more pronounced in the DEM simulations. From the figures it emerges that both the horizontal thrusts and the deflection profiles obtained by the DEM simulations compare well with the results obtained by FDM where a dense mesh was used (25 x 25 for each block).

Since the DEM analyses are in agreement with FDM simulations of Tsesarsky & Talesnick, (2007), obviously the DEM simulations cannot provide a closer fit to the experimental measurements than the FDM. The main discrepancies concern the magnitude of the thrust that is ~30% lower than the experimental measurements and the displacements at both midspans and abutments which are under-predicted as for the FDM of Tsesarsky & Talesnick (2007). Assuming that the problem does not lie with the capabilities of the numerical codes, a strong possibility is that the contact models of Eqs. (1) and (2) are not sufficiently accurate.

4.2 Verification of line of thrust for DEM model with rigid blocks and deformable joints

In the study of masonry structures (Heyman, 1997; Timoshenko, 1983), the line of thrust under the structure's self-weight is known to assume the catenary shape of Hooke's inverted chain (refer to Lamb (1916) for equations). On the other hand, in the rock engineering literature, the line of thrust of a voussoir beam is assumed to be of parabolic shape (Beer & Meek, 1982; Brady & Brown, 2004; Diederichs & Kaiser, 1999a; Sofianos, 1996; Sofianos & Kapenis, 1998). So the contact points between blocks were fitted using both a uniform catenary curve and a parabola for gravitational accelerations of 10 g and 40 g to extrapolate the line of thrust for the beams (see Figure 7). Looking at the Figure, it emerges that both catenary curve and parabola fit the contact points equally well and there

is very little difference between them. Also it emerges that the DEM results compares well with the experimental measurements deduced from the strain gauges.

Diederichs & Kaiser (1999a) considered the line of thrust obtained by UDEC (Itasca, 1996) for non-deformable abutments unrealistic because they were expecting, according to their analytical solutions, that the contact force between beam and abutment to be not located at the lower corner. This has been subsequently experimentally confirmed by centrifuge tests performed by Talesnick et al. (2007). This issue is probably due to the contact detection algorithm employed in UDEC and was not observed in our analyses.

4.3 Results for the new contact model

The parameters and models employed in each figure are summarised in Table 3. From Figure 5 it emerges that the more accurate contact models have a negligible influence on the magnitude of horizontal thrust for the full-block beam. The discrepancies between the load cell and strain gauge measurements are still not resolved (Talesnick et al., 2007). However, using the proposed more accurate contact model in the normal direction (Eq. (4)) while keeping the shear stiffness model (Eq. (2)) of Tsesarsky & Talesnick (2007), the predicted deflections of the DEM simulations agree better with the experimental measurements (see Figure 8). Using also the more refined shear contact model in Eq. (8), the calculated shear displacements at the abutment (Figure 9) are slightly larger compared to those in Figure 8 simulated using the simpler model in Eq. (2). Overall, this resulted in an overprediction of approximately 28% at the midspan, averaged among the three sets of tests at 40 g (Figure 9 (a), (b), (c)), by comparison to the contact models of Tsesarsky & Talesnick (2007) (Eq. (1) and Eq. (2)) which resulted in an underprediction of approximately 40% on average (see Table 3 for summary of comparison).

Note that the displacements at the abutment were under-predicted by the DEM simulations (Figure 9). Poor predictions of shear displacements by the advanced shear model (Eqs. (7) and (8)) are largely due to the lack of experimental shear data for model calibration at higher normal stresses under which the experiments were conducted; the shear tests for stiffness calibration was carried out up to a normal stress of 0.023 MPa, in contrast to centrifuge tests for which the approximated normal stresses were up to 0.5 MPa for the full-block beam and 1.0 MPa for the half-block beam.

5. Conclusions

The paper presented a rigorous DEM exercise which showcases the importance of using accurate contact laws to predict actual displacements resulting from rock block interactions. The discrepancies observed previously between the DEM and FLAC analyses (see Figure 6) using the same contact constitutive models are much smaller by comparison to the discrepancies using less accurate contact constitutive models; the DEM predictions improved significantly when more accurate contact constitutive models were used. The calibration of the models in this paper shows the possibility of using customised approaches to derive specific contact models for the DEM, which can be applied in other rock engineering applications.

The second conclusion is that the DEM with the contact detection algorithm of Boon et al. (2012) is capable of correctly calculating the line of thrust for jointed single layer rock beams subject to gravitational acceleration.

Acknowledgements

The experimental data in Talesnick et al. (2007) was maintained online by Dr. Mark Talesnick at his personal homepage in Talesnick (2006), when this study was undertaken.

References

Alejano, L. R., Taboada, J., GarcÃa-Bastante, F., & Rodriguez, P. (2008). Multi-approach back-analysis of a roof bed collapse in a mining room excavated in stratified rock. International Journal of Rock Mechanics and Mining Sciences, 45(6), 899-913.

Bakun-Mazor, D., Hatzor, Y. H., & Dershowitz, W. S. (2009). Modeling mechanical layering effects on stability of underground openings in jointed sedimentary rocks. International Journal of Rock Mechanics and Mining Sciences, 46(2), 262-271.

Barla, G., Monacis, G., Perino, A., & Hatzor, Y. H. (2010). Distinct element modelling in static and dynamic conditions with application to an underground archaeological site. Rock Mechanics & Rock Engineering, *43*(6), 877-890.

Beer, G., & Meek, J. L. (1982). DESIGN CURVES FOR ROOFS AND HANGING-WALLS IN BEDDED ROCK BASED ON â€³VOUSSOIRâ€³ BEAM AND PLATE SOLUTIONS. Transactions of the Institution of Mining and Metallurgy, Section A: Mining Technology, 91, 18-22. Retrieved from www.scopus.com

Beer, G., Meek, J. L., & Cowling, R. (1981). Prediction of behaviour of shale hangingwalls in deep underground excavations. 5th I.S.R.M.Symposium, , D45-51. Retrieved from www.scopus.com

Boon, C.W. (2013) The Distinct Element Modelling of Jointed Rock Masses: Algorithms and Their Verification. DPhil Thesis. University of Oxford.

Boon, C.W., Houlsby, G.T., Utili, S. (2012) A new algorithm for contact detection between convex polygonal and polyhedral particles in the discrete element method, *Computers & Geotechnics*, Vol. 44, 73-82.

Boon CW, Houlsby GT, Utili S. (2013) A new contact detection algorithm for three dimensional non-spherical particles. *Powder Technology*, SI on DEM, **248**: 94-102.

Boon CW, Houlsby GT, Utili S. (2014a). Designing tunnel support in jointed rock masses via the DEM. *Rock mechanics and rock engineering,* DOI: 10.1007/s00603-014-0579-8 (on-line).

Boon CW, Houlsby GT, Utili S. (2014b). New insights in the 1963 Vajont slide using 2D and 3D Distinct Element Method analyses. *Geotechnique,* **64**(10): 800-816.

Brady, B. H. G., & Brown, E. T. (1993). Rock mechanics for underground mining. Rock Mechanics for Underground Mining, Retrieved from www.scopus.com

Diederichs, M. S., & Kaiser, P. K. (1999a). Stability of large excavations in laminated hard rock masses: The voussoir analogue revisited. International Journal of Rock Mechanics and Mining Sciences, 36(1), 97-117. Retrieved from www.scopus.com

Diederichs, M. S., & Kaiser, P. K. (1999b). Tensile strength and abutment relaxation as failure control mechanisms in underground excavations. International Journal of Rock Mechanics and Mining Sciences, 36(1), 69-96. Retrieved from www.scopus.com

Evans, W. H. (1941). The strength of undermined strata. Trans.Inst.Min.Metall., 50(50), 475-532.

~~Fayol, M. (1885). Sur les movements de train provoques par l'exploitation des mines. Bull. Soc. Indust. Min, 14, p. 818.~~

Hatzor, Y. H., & Benary, R. (1998). The stability of a laminated voussoir beam: Back analysis of a historic roof collapse using DDA. International Journal of Rock Mechanics and Mining Sciences, 35(2), 165-181. Retrieved from www.scopus.com

Hatzor, Y. H., Wainshtein, I., & Bakun Mazor, D. (2010). Stability of shallow karstic caverns in blocky rock masses. International Journal of Rock Mechanics and Mining Sciences, 47(8), 1289-1303.

Heyman, J. (1997). The Stone Skeleton: Structural Engineering of Masonry Architecture. Cambridge University Press, pp. 172.

Houlsby, G. T. (2009). Potential particles: a method for modelling non-circular particles in DEM. Computers and Geotechnics, 36(6), 953-959.

Itasca (2000). Fast Lagrangian Analysis of Continua – FLAC, ver. 4. Itasca Consulting Group Inc: Minneapolis, 2000.

Itasca (1996). Universal Distinct Element Code – UDEC, ver. 3. Itasca Consulting Group Inc: Minneapolis.

Kozicki, J. & Donzé, F. V. (2008). A new open-source software developed for numerical simulations using discrete element methods. Computer Methods in Applied Mechanics and Engineering, 197(49-50), 4429-4443.

Lamb, H. (1916). Statics: including hydrostatics and the elements of the theory of elasticity. Cambridge University Press, pp. 341.

Nomikos, P. P., Sofianos, A. I., & Tsoutrelis, C. E. (2002). Structural response of vertically multi-jointed roof rock beams. International Journal of Rock Mechanics and Mining Sciences, 39(1), 79-94.

Sofianos, A.I. (1996). Analysis and design of an underground hard rock Voussoir beam roof. International Journal of Rock Mechanics and Mining Science, Vol. 33, No. 2, 153-166.

Sofianos, A. I., & Kapenis, A. P. (1998). Numerical evaluation of the response in bending of an underground hard rock voussoir beam roof. International Journal of Rock Mechanics and Mining Sciences, 35(8), 1071-1086.

Talesnick, M. L. (2006). Use of voissoir beam centrifuge data for the validation of numerical frameworks and constitute models, from http://www.technion.ac.il/~talesnik/Voussoir%20validation%20Notes.htm

Talesnick, M. L. (2007). Determination of shear interface parameters between rock blocks for centrifuge modeling. Rock Mechanics and Rock Engineering, 40(4), 405-418.

Talesnick, M. L., Ya'Acov, N. B., & Cruitoro, A. (2007). Modeling of a multiply jointed voussoir beam in the centrifuge. Rock Mechanics and Rock Engineering, 40(4), 383-404.

Timoshenko, S. P. (1983). History of Strength of Materials. Dover: New York. Reprint Edition. Pp. 452.

Tsesarsky, M., & Talesnick, M. L. (2007). Mechanical response of a jointed rock beam - numerical study of centrifuge models. International Journal for Numerical and Analytical Methods in Geomechanics, 31(8), 977-1006.

Tsesarsky, M., & Hatzor, Y. H. (2006). Tunnel roof deflection in blocky rock masses as a function of joint spacing and friction - A parametric study using discontinuous deformation analysis (DDA). Tunnelling and Underground Space Technology, 21(1), 29-45.

Tsesarsky, M. (2012). Deformation mechanisms and stability analysis of undermined sedimentary rocks in the shallow subsurface. Engineering Geology, 133-134, 16-29.

Appendix A– Stress-update algorithm (shear direction)

The total shear displacement increment, **du**, consists of elastic and plastic components, i.e. $\mathbf{du}_e$ and $\mathbf{du}_p$, such that:

$$\mathbf{du} = \mathbf{du}_e + \mathbf{du}_p \tag{A.1}$$

from which the increment of plastic displacement can be expressed as:

$$\mathbf{du}_p = \mathbf{du} - \frac{\mathbf{F}_i - \mathbf{F}_0}{K_s} \tag{A.2}$$

where $\mathbf{F}_i$ and $\mathbf{F}_0$ are the shear forces at the current and previous time step and K_s is the shear stiffness (units: N/m).

For the case when the coefficient of friction μ is modelled as strain hardening or strain softening, it is useful to denote $\mu = g(\beta)$, so that, μ, is a function g of an internal state variable β. Then, define the increment of the internal state variable $d\beta$ as a scalar product of $\mathbf{du}_p$ to the power of half:

$$d\beta = (\mathbf{du}_p \mathbf{du}_p)^{1/2} \tag{A.3}$$

so that

$$\beta_i = \beta_0 + d\beta \tag{A.4}$$

where β_i and β_0 are the values of the internal state variable at the current and previous time step respectively. The solving of the equations in the stress-update algorithm assumes

a dependency of the friction coefficient on the plastic shear displacements instead of the total shear displacements in Eq. (8) for calibration convenience (this very slightly delays the reaching of the asymptote for the exponential decay function in Eq. (8)). By assuming that the plastic strain increment is in the direction of current shear stress,

$$\mathbf{du}_{\mathrm{p}} = \Lambda \mathbf{F}_{\mathrm{i}} \tag{A.5}$$

the state variable β_i can be expressed as:

$$\beta_i = \beta_0 + \Lambda(\mathbf{F}_i \mathbf{F}_i)^{1/2} \tag{A.6}$$

and the shear force as:

$$\mathbf{F}_{\mathrm{i}} = \frac{K_{\mathrm{s}} \mathbf{du} + \mathbf{F}_0}{K_{\mathrm{s}} \Lambda + 1} \tag{A.7}$$

Define the yield surface as:

$$f = (\mathbf{F}_{\mathrm{i}} \mathbf{F}_{\mathrm{i}})^{1/2} - \mu_{\mathrm{i}} F_{\mathrm{n}} \tag{A.8}$$

where F_{n} is the magnitude of normal force at the contact and μ_{i} is the corresponding friction coefficient at the current time step.

In the stress update algorithm, the plastic multiplier Λ is sought so that the shear force $\mathbf{F}_{\mathrm{i}}$ is on the yield surface, i.e. $f = (\mathbf{F}_{\mathrm{i}} \mathbf{F}_{\mathrm{i}})^{1/2} - \mu_{\mathrm{i}} F_{\mathrm{n}} = 0$. To bracket Λ on the yield surface, a pair of values of Λ are needed, i.e. values that result in negative and positive values of *f*. One of the bracketing ends of Λ can be taken as 0, i.e. for the case of full elastic update outside the yield surface. The other bracketing value for Λ should result in the shear stress being inside the yield surface. As a first approximation, it can be taken as $\Lambda = \dfrac{\mathbf{du}}{\mathbf{F}_0}$. If this shear stress is outside the yield surface, Λ is iteratively increased until it lies inside the yield surface. With a pair of bracketing range for Λ, the remaining unknowns in the yield

surface (Eq. (A.8)) are the shear force $\mathbf{F}_{\mathrm{i}}$ and the current friction coefficient μ_{i}. The first can be calculated from Eq. (A.7), and the second from $\mu_{\mathrm{i}} = g(\beta_{\mathrm{i}})$ where β_{i} can in turn be calculated from Eq. (A.6). Bracketing algorithms can be used for this purpose.

Tables and Figures

Table 1. Mechanical properties of the blocks after Talesnick et al. (2007).

Properties	Values
Density	1207 kg/m3
Deformability of intact block	5600 MPa
Friction angle of interface	40°

Table 2. Joint properties adopted in the DEM simulations and results of comparison with FLAC

No.	Model	k_n (GPa/m)	k_s (GPa/m)	Discrepancy at midspan, (DEM-FLAC)/FLAC
1	full-block	10	1	-16% at 40 g
2	full-block	linear model - Eq. (3)	linear model - Eq. (2)	-12% at 40 g
3	half-block	10	1	-11% at 90 g

*Negative indicates underprediction

Table 3. Summary of the models employed in DEM simulations and results of comparison with experimental measurements

Figure No.	Experiment reference, data downloaded from website (Talesnick, 2006)	k_n	k_s	Discrepancy at midspan, (DEM-EXP)/EXP, based on new contact models (left columns)	Discrepancy at midspan, (DEM-EXP)/EXP, linear model proposed by Tsesarsky & Talesnick (2007) (Eqs. 2 & 3)
9 (a)	full-block, 180-C0 (same experiment setup)	linear model (half stiff) Eq. (4)	continously yielding model - Eqs. (7) & (8)	13.8% at 40 g	-46.7% at 40 g
9 (b)	full-block, 180-D (same experiment setup)	linear model (half stiff) Eq. (4)	continously yielding model - Eqs. (7) & (8)	40.0% at 40 g	-34.4% at 40 g
9 (c)	full-block, 180-E (same experiment setup)	linear model (half stiff) Eq. (4)	continously yielding model - Eqs. (7) & (8)	30.0% at 40 g	-39.0% at 40 g
N/A	half-block, 180-3	linear model (half stiff) Eq. (4)	continuously yielding model - Eqs. (7) & (8)	-32% at 90g	-68.0% at 90 g

*The measured deflection profiles of experiment 180-C0 and 180-D are not symmetrical, and the midspan blocks with the larger deflections were used (note that Tsesarsky & Talesnick (2007) used the smaller midspan block from 180-D as benchmark, which is also the smallest among all three tests)

*Positive indicates overprediction, and negative indicates underprediction

*Refer to Boon (2013) for plot of deflection profiles

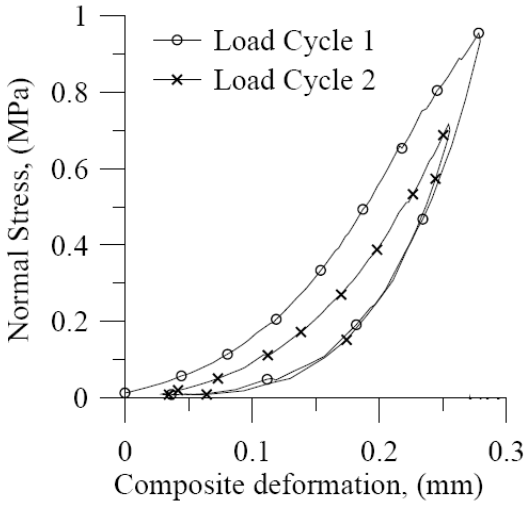

(a)

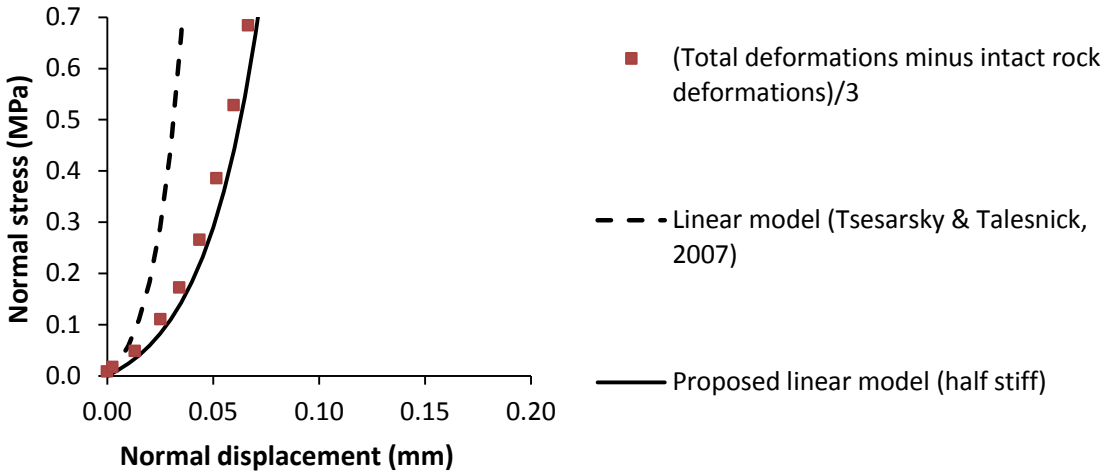

(b)

Figure 1. Stress-deformation of load-unload cycles for (a) uniaxial compression of a three-block column (after Fig. 14 in Talesnick et al., 2007, with kind permission from Springer Science and Business Media), (b) derived contact model from Fig (a) after deducting the deformations of the intact rock material and dividing it by three (total number of equivalent rock joint contacts including the topmost and bottommost block interface in the uniaxial test of the three-block column).

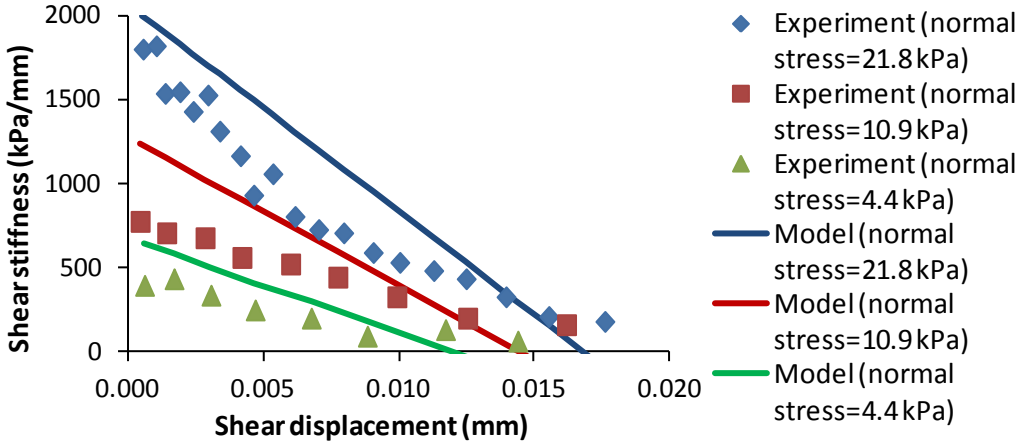

Figure 2. Shear stiffness as a function of shear displacement at different normal stress. The experimental shear stiffness was taken from the 2nd loading cycle: proposed model (Eq. (5)) plotted against experimental data deduced from Fig. 5(c) in Talesnick (2007)

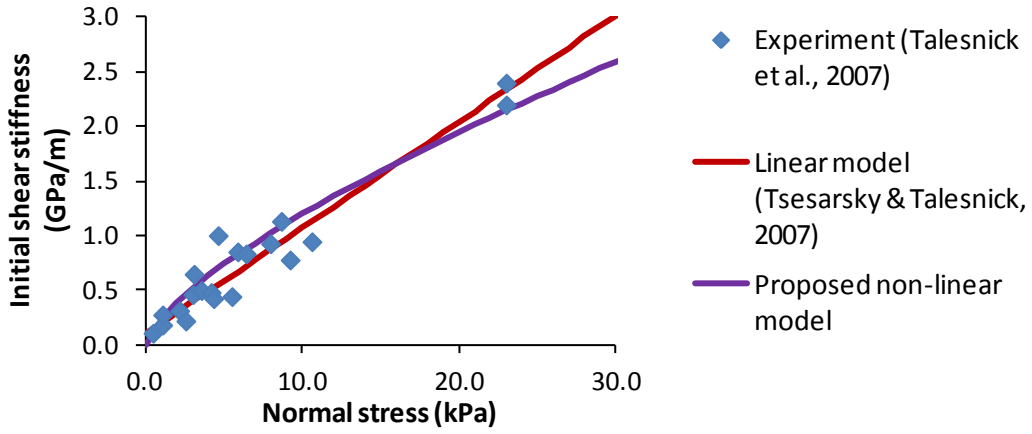

Figure 3. Initial shear stiffness as a function of normal stress. The proposed model Eq. (7) is plotted against experimental values and the model (Eq. (2)) proposed by Tsesarsky & Talesnick (2007)

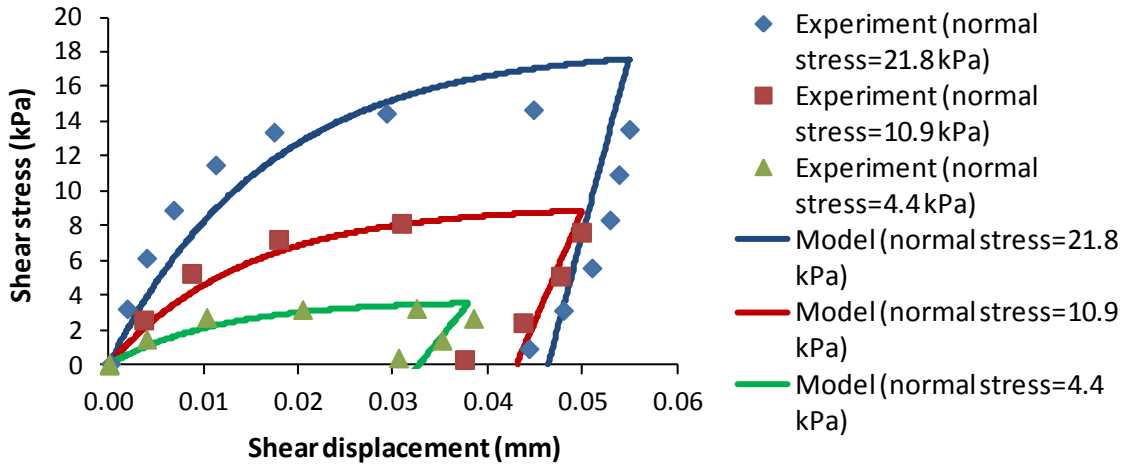

Figure 4. Shear stress versus shear displacement at different normal stress: proposed model (Eq. (8)) and experimental data deduced from Fig. 4(b) in Talesnick (2007)

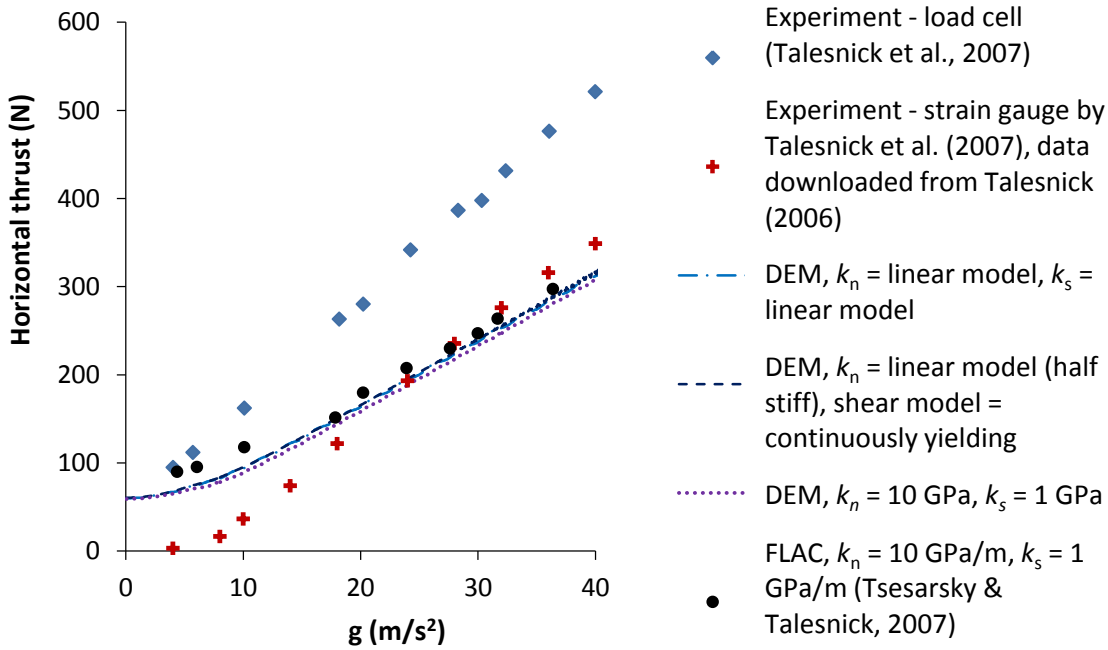

Figure 5. Comparison of thrust build-up of the full-block and between DEM simulations and experiments (blue diamonds) carried out by Talesnick et al. (2007). The forces estimated from strain gauges were obtained from Test 180-E (Talesnick, 2006). The magnitude (417 N derived from strains) stated in Fig. 20 in Talesnick et al. (2007), seems to be inconsistent with the strain plots in Fig. 20, which is closer to approximately 349 N. There is negligible

difference in terms of horizontal thrust predictions among the three DEM simulations presented here.

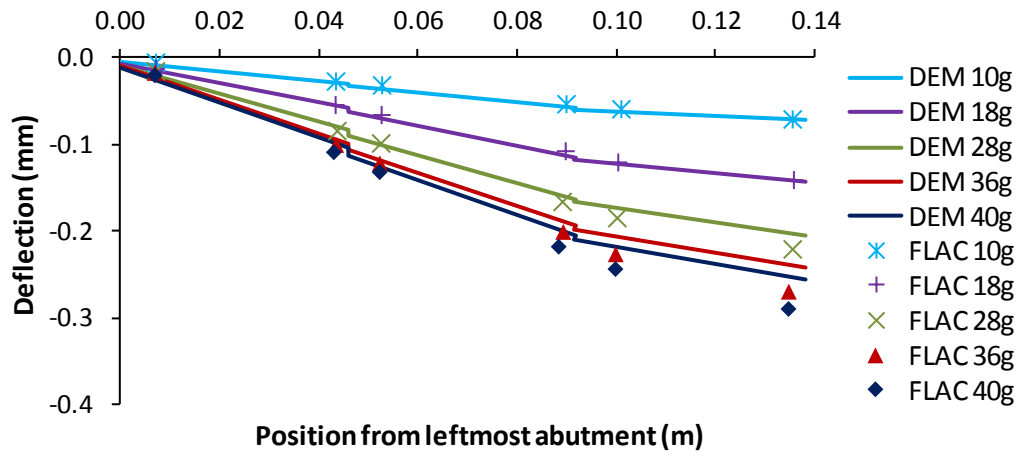

Figure 6. DEM displacement profile in comparison with FLAC simulations by Tsesarsky & Talesnick (2007): full-block model with both k_n and k_s = linear model

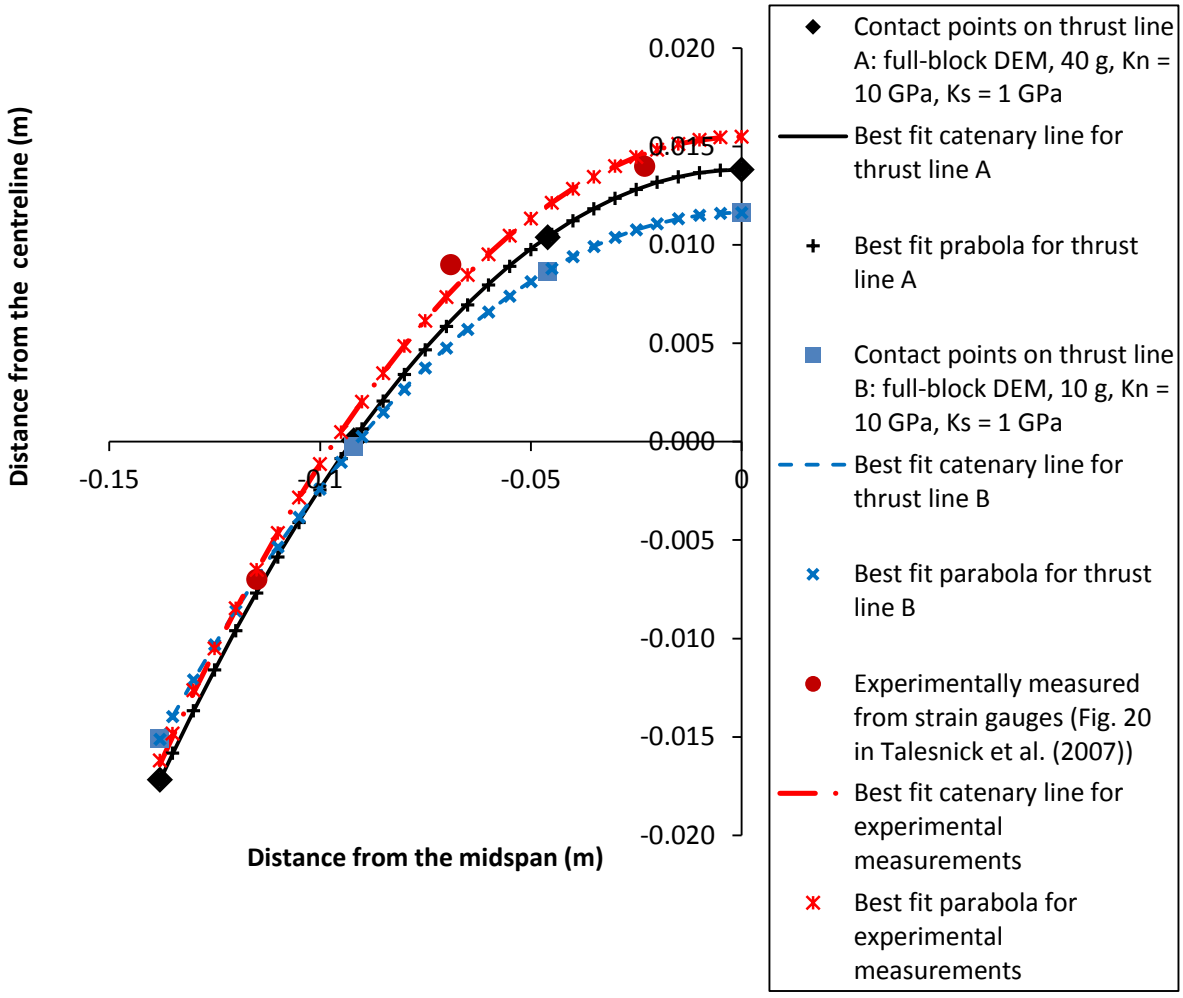

Figure 7. Catenary line fit for contact points obtained from DEM analysis at 10 g and 40 g for the full-block model. Note that the line of thrust obtained from strain gauges are not distinguished between different gravitational accelerations due to negligible differences (Fig. 20 in Talesnick et al. (2010)). For experimental measurements, the best fit lines are assumed to pass through 0.0155 m from the centreline at the midspan. Note that from Figure 5, similar conclusions can be drawn for the other contact models used in paper.

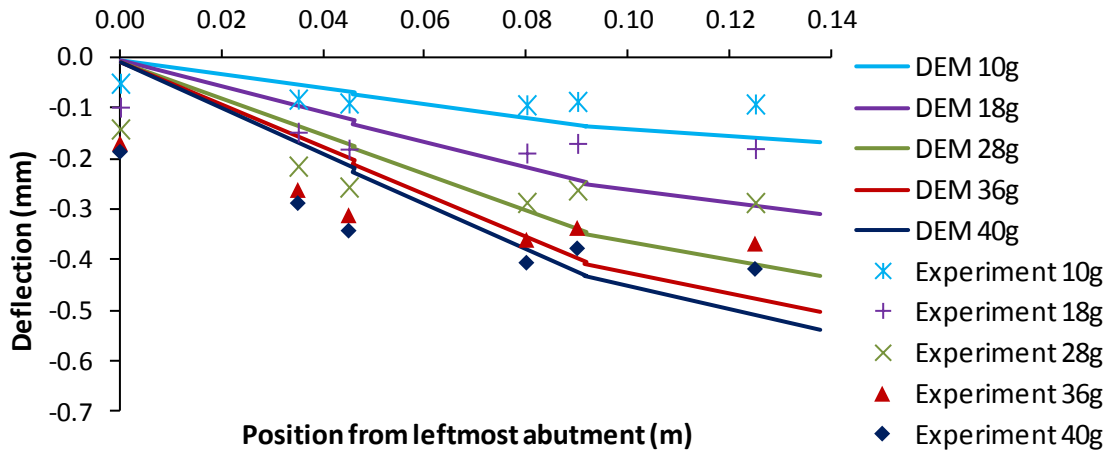

Figure 8. . DEM displacement profile for the full-block and, k_n = linear model with half stiffness Eq. (4) and k_s = linear model Eq. (2) in comparison with experiments carried out by Talesnick et al. (2007). Experimental deflections were measured from LVDT (Test 180-E for the full-block model).

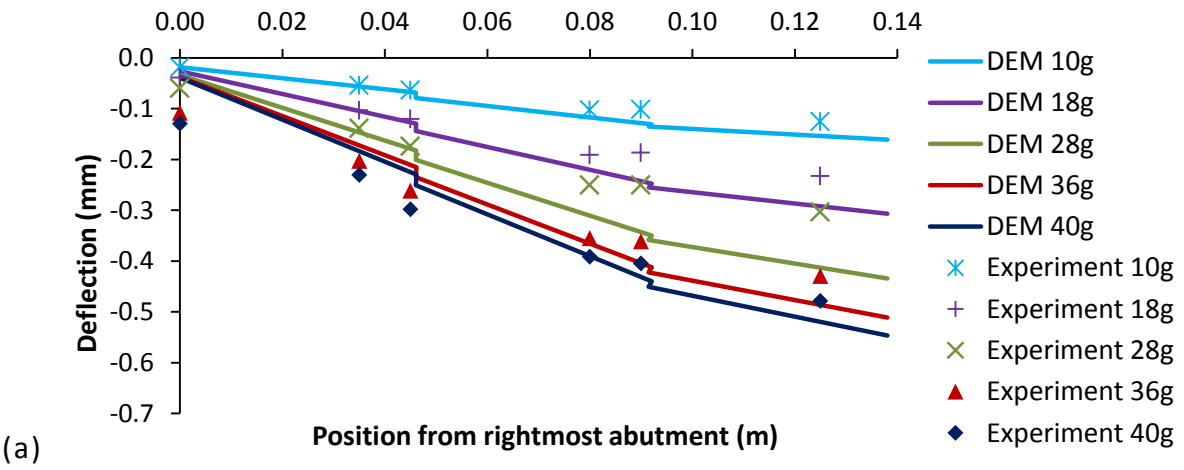

(a)

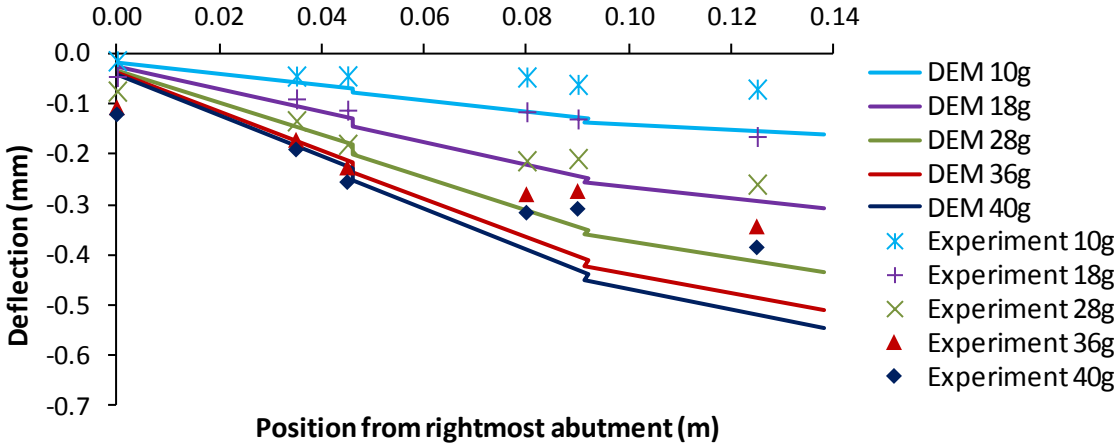

(b)

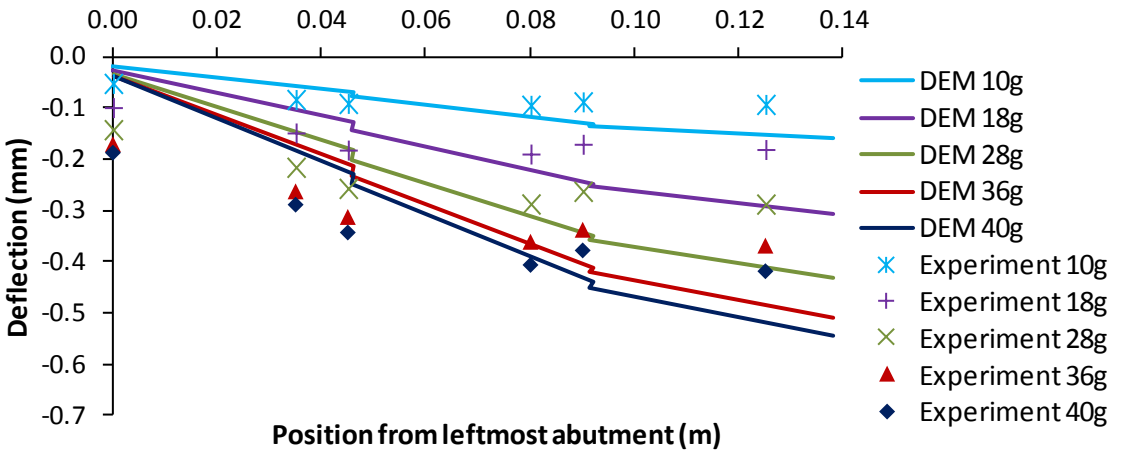

(c)

Figure 9. DEM displacement profile for the full-block model, k_n = linear model with half stiffness Eq. (4) and k_s = continuously yielding model Eq. (8) in comparison with experiments carried out by Talesnick et al. (2007). Experimental deflections were measured from LVDT: (a) 180-C0, (b) 180-D, (c) 180-E